


Zeonex-based asymmetrical terahertz photonic crystal fiber for multichannel communication and polarization maintaining applications

MD. SAIFUL ISLAM,^{1,*}  JAKEYA SULTANA,^{1,2} ALEX DINOVITSER,¹ MOHAMMAD FAISAL,³ MOHAMMAD RAKIBUL ISLAM,² BRIAN W.-H. NG,¹ AND DEREK ABBOTT¹

¹The University of Adelaide, School of Electrical & Electronic Engineering, Adelaide 5005, Australia

²Islamic University of Technology, Electrical & Electronic Engineering, Gazipur 1704, Bangladesh

³Bangladesh University of Engineering & Technology, Electrical & Electronic Engineering, Dhaka 1000, Bangladesh

*Corresponding author: mdsailful.islam@adelaide.edu.au

Received 10 November 2017; revised 23 December 2017; accepted 24 December 2017; posted 2 January 2018 (Doc. ID 313178); published 25 January 2018

We report on the design, in-depth analysis, and characterization of a novel elliptical array shaped core rectangular shaped cladded photonic crystal fiber (PCF) for multichannel communication and polarization maintaining applications of terahertz waves. The asymmetrical structure of air holes in both core and cladding results in increased birefringence, while a compact geometry and different cladding air hole size makes the dispersion characteristic flat. The modal characteristics of the PCF are calculated using a finite element method. The simulated results show a near-zero dispersion flattened property of ± 0.02 ps/THz/cm, high birefringence of 0.063, low effective material loss of 0.06 cm⁻¹, and negligible confinement loss of 5.45×10^{-13} cm⁻¹ in the terahertz frequency range. Additionally, the core power fraction, effective area, physical attributes, and potential fabrication possibilities of the fiber are discussed. © 2018 Optical Society of America

OCIS codes: (050.5298) Photonic crystals; (060.2420) Fibers, polarization-maintaining; (060.2330) Fiber optics communications; (060.2430) Fibers, single-mode.

<https://doi.org/10.1364/AO.57.000666>

1. INTRODUCTION

Terahertz radiation, also called sub-millimeter-wave radiation, consists of electromagnetic waves within the 0.1–10 THz band. As the terahertz regime lies between the infrared and microwave ranges, it carries characteristics from both of them. Over the last few decades, the field of terahertz radiation has increased tremendously because of its potential applications in different fields. Nowadays imaging [1–4], sensing [5,6], pharmaceutical drug testing [7], communication [8,9], astronomy [10], biomedical engineering for diagnosis and detection [11–14], and hazardous substances [15] are largely dependent on terahertz photonic crystal fiber (PCF). Moreover, terahertz can be used for skin cancer and breast cancer detection that is more suitable than x rays because it is non-ionizing [4,16,17]. Though the benefits of terahertz waves are remarkable, their generation has remained a challenge [18,19]. To fill the gap, researchers are working towards technologies for appropriate terahertz sources, low loss transmission media, and efficient detectors [18,20]. While terahertz sources and detectors are available for commercial use, researchers are now focusing on the design and implementation of efficient terahertz

waveguides [21]. To meet the requirements of a novel terahertz system with high density integration requires a compact terahertz waveguide with higher birefringence, ultra-flattened dispersion as well as low loss along with increased core power fraction. To achieve these particular demands, various types of waveguides have already been proposed. Among them, metallic wire [22], dielectric metal-coated tube [23], plastic fiber [24], polymer Bragg fiber [25], polystyrene foam [26], hollow core fiber [27], and solid core fiber [28] have been reported. However, these all are problematic due to their undesirable narrow band operation, higher material loss, high bending loss, and strong coupling with the surrounding environment.

Therefore, greater attention is now focused on porous core fibers [2,29–40] where the waveguide parameters such as core diameter, pitch size, air filling fraction, air hole radius, and frequency can be determined by design. Furthermore, in a PCF, by selecting the geometrical parameters it is possible to achieve low material absorption loss, low confinement loss, low dispersion variation, high birefringence, and high core power fraction [25].

To use a fiber efficiently in multichannel communication and polarization maintaining applications, a number of

PCFs have been proposed in recent years [29–33]. In 2009, an experimental study on dispersion properties of a porous core fiber was investigated by Atakaramians *et al.* [41]. They also investigated different shapes of PCF structure including circular and rectangular shapes to obtain specific characteristics of birefringence and dispersion [42]. Later, in order to obtain high birefringence and flat dispersion a slotted core circular cladded PCF was proposed [34]. They obtained a high birefringence of 0.075, but with a high dispersion variation ± 0.5 ps/THz/cm. An oligo-porous core PCF with asymmetric hexagonal lattice was also proposed by Wu *et al.* [37]; however, it failed to improve birefringence and the dispersion property of the fiber. Recently, Luo *et al.* proposed a square lattice PCF for flattened dispersion and high birefringence [43]. They obtained a birefringence of 0.063 with dispersion variation of ± 0.12 for x -polarization mode and ± 0.08 for y -polarization mode.

Therefore, after analyzing the literature for flattened dispersion and highly birefringent fiber it is found that there is a large scope for PCF improvement in the case of dispersion variation and birefringence.

In this paper, in a Zeonex substrate we propose a novel PCF consisting of a rectangular shaped air hole based cladding and an elliptical array of air hole based core. The aim is to flatten the dispersion and increase birefringence with the reduction of confinement loss. One of the greatest advantages of the proposed PCF is its simplicity, and thus fabrication is feasible using the state-of-the-art techniques.

2. PHYSICAL INSIGHT OF THE PROPOSED WAVEGUIDE

The finite element method (FEM) based software Comsol 4.3b is used to design the structure of the proposed waveguide. The proposed PCF structure combines an array of elliptical air holes in the core together with a slotted cladding structure, where asymmetries in both the core and cladding are utilized to increase the birefringence.

In the cladding region of Fig. 1, the rectangular slot lengths are defined as L_1, L_2, L_3 , and L_4 as indicated. The defined lengths are 1200, 3000, 2700, and 2000, and 1000 μm , respectively. Here, W and P represent the slot width and pitch distance (center to center distance between air holes) that are the same for each rectangular air hole. Note that during standard fabrication, $\pm 2\%$ variation of the global diameter of a PCF

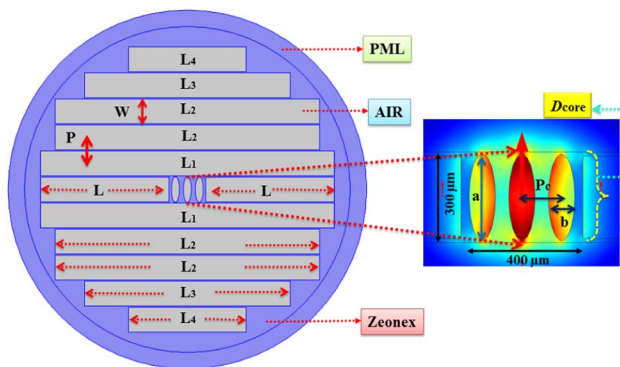


Fig. 1. Cross section of the proposed slotted lattice PCF.

can occur [6]. Thus considering the fabrication difficulties, the pitch P and slot width W are fixed at 280 and 270 μm , respectively.

The core region of the PCF is defined as D_{core} . The major axis length and minor axis length of the elliptical shaped air holes inside D_{core} are defined as a and b . Considering the fabrication conditions, we fixed a maximum major axis length of 142 μm , and by doing such we are able to increase the index difference between the polarization modes and thus increase the birefringence. However, we varied the minor axis length b to investigate the fiber characteristics in b . The maximum allowable minor axis length is 63 μm , and further increase may overlap the air holes and create fabrication difficulties. Therefore, the core pitch distance P_c was set to 65 μm to allow sufficient distance between the elliptical air holes. In our proposed PCF the core length is 400 μm while the core width is 300 μm . The total fiber diameter including the perfectly matched layer (PML) is 3.9 mm.

During simulation, we select *extremely fine* mesh in Comsol 4.3b that divides the whole PCF into a large number of mesh elements that increases the accuracy of fiber characterization. We found that the total number of elements composing the mesh is 27,458 and the average element quality is 0.91, so the computational error by using Comsol is less than 0.1%. The propagation constants, field distributions, and power distributions of guiding modes are calculated by applying proper boundary conditions. From there, we are able to calculate other parameters such as effective area, power fraction, effective material loss (EML), and dispersion. The different boundary conditions (i) PML, (ii) perfect electric conductor (PEC), and (iii) perfect magnetic conductor (PMC) are shown in Fig. 2. To ensure near-zero reflection, a PML is set as the outer boundary of the fiber that is 10% of the total fiber radius [4,6,9]. The PMC ensures that the electric field is symmetric and the

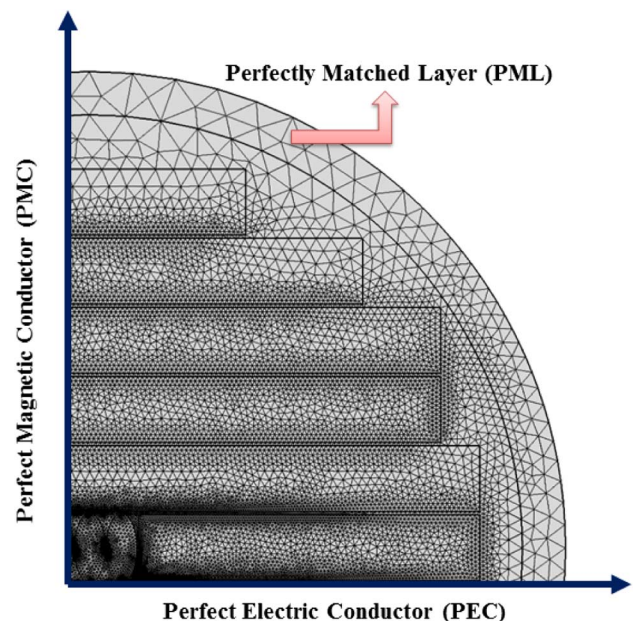


Fig. 2. Mesh of the proposed PCF with different boundary conditions.

magnetic field is asymmetric, whereas under the PEC condition the electric field is asymmetric and the magnetic field is symmetric in the direction of propagation along the waveguide [44]. Moreover, the refractive index of the core is greater than the cladding; thus, light pulses through the fiber will be guided by modified total internal reflection (MTIR) [33,43].

Among the available polymer materials [45–48], Cyclo Olefin Polymer (COP), commercially known as Zeonex, is selected as the background material for the proposed PCF. Zeonex has a number of advantages, including constant refractive index of 1.53 in the terahertz frequency range, negligible material dispersion, high glass transition temperature T_g , low absorption loss of 0.2 cm^{-1} , negligible water absorption ($<0.1\%$), high biocompatibility, and excellent chemical resistance even at elevated temperatures [47].

In optical communication systems, multiplexing techniques came into existence to increase the information carrying capacity of a channel. However, the main limiting factors are the dispersion and fiber nonlinearity. In a conventional silica based fiber, dispersion increases with wavelength and thus different optical channels suffer different amounts of pulse broadening. One of the solutions is to use a dispersion compensator in reshaping the signals, but it requires repeaters after a particular distance [49]. To overcome these difficulties, fibers with low finite dispersion with negligible dispersion flatness are required. The flat dispersion property helps the number of input signals of a multichannel communication system in being transmitted through the fiber with minimum pulse broadening and thus increases the channel capacity.

In designing the PCF, our main motivation is to flatten the dispersion characteristic. Dispersion originates from the waveguide structure, as well as from the material itself. Note that Zeonex exhibits negligible material dispersion in the terahertz frequency range; therefore the effect of material dispersion is ignored. Hence we calculate the waveguide dispersion that mainly depends on the geometrical structure of the fiber. Waveguide dispersion of a fiber can be characterized by the following equation [43]:

$$\beta_2 = \frac{2}{c} \frac{dn_{\text{eff}}}{dw} + \frac{w}{c} \frac{d^2 n_{\text{eff}}}{dw^2}, \text{ ps/THz/cm}, \quad (1)$$

where β_2 is the dispersion parameter, ω indicates the angular frequency, c represents the velocity of light in air, and n_{eff} is the effective refractive index of the fiber.

Birefringence is another important parameter that needs to be considered for polarization maintaining terahertz applications. It mainly depends upon the air hole geometry in the fiber. The greater the asymmetry in the x - and y -polarization mode, the higher the birefringence. It can be calculated by the equation [38]

$$B = |n_x - n_y|, \quad (2)$$

where B represents the birefringence, and n_x and n_y are the refractive indices of the orthogonal polarization mode.

Besides flattened dispersion and high birefringence, it is also important to take care of the loss properties of the PCF. The two most important loss mechanisms are EML and confinement loss. The EML of a PCF can be characterized by the equation [43]

$$\alpha_{\text{eff}} = \sqrt{\frac{\epsilon_0}{\mu_0}} \left(\frac{\int_{\text{mat}} n_{\text{mat}} |E|^2 \alpha_{\text{mat}} dA}{\left| \int_{\text{all}} S_z dA \right|} \right), \text{ cm}^{-1}, \quad (3)$$

where α_{eff} represents the EML, μ_0 and ϵ_0 designate the permeability and permittivity in air, respectively, α_{mat} and n_{mat} represent the bulk absorption loss and refractive index of Zeonex in that order, and S_z denotes the z component of the Poynting vector.

Confinement loss of a fiber determines the length of signal transmission in a terahertz optical waveguide. It basically depends upon the core porosity and the structure of the cladding. It can be characterized by the equation [30]

$$L_c = \left(\frac{4\pi f}{c} \right) \text{Im}(n_{\text{eff}}), \text{ cm}^{-1}, \quad (4)$$

where L_c characterizes the confinement loss, and $\text{Im}(n_{\text{eff}})$ represents the imaginary part of the complex effective refractive index.

The amount of power propagating inside the core region can be characterized by the term core power fraction. It can be estimated by the equation [43]

$$\eta' = \frac{\int_X S_z dA}{\int_{\text{all}} S_z dA}, \quad (5)$$

where the integration in the numerator is over the region of interest and the integration in the denominator is over the whole fiber region.

The area covered by electromagnetic waves inside the core region of a fiber can be characterized by the term effective area. It is characterized by A_{eff} , as follows [30]:

$$A_{\text{eff}} = \frac{\left[\int I(r) r dr \right]^2}{\left[\int I^2(r) dr \right]^2}, \quad (6)$$

where $I(r) = |E_t|^2$ indicates the intensity of the electric field distribution across the cross section of the fiber.

3. FABRICATION POSSIBILITIES OF ELLIPTICAL ARRAY SHAPED CORE SLOTTED-CLAD PCF

The proposed fiber consists of an elliptical array inside a slotted air hole based lattice. Note that by using an extrusion technique, slotted structured air holes have already been fabricated by Atakaramians *et al.* [42,50]. In addition, the elliptical shaped air holes have been fabricated by Issa *et al.* [51]. Moreover, using the methyl methacrylate (MMA) monomer polymerization method, Liu *et al.* [52] fabricated elliptical shaped air holes. A recently published paper on PCF showed that the elliptical shaped air holes can be fabricated using existing fabrication techniques [53]. In addition, micro-structured polymer optical fiber with asymmetric air holes is feasible using 3D printing technology [54,55].

4. NUMERICAL RESULTS AND DISCUSSION

The mode field distribution of the proposed PCF at different core air hole width is shown in Fig. 3. It can be observed that light is well confined into the core area. The effective refractive index value at the x -polarization mode is 1.1374.

Moreover, as the PCF is asymmetrical in structure, the effective refractive index for the x -polarization mode is slightly

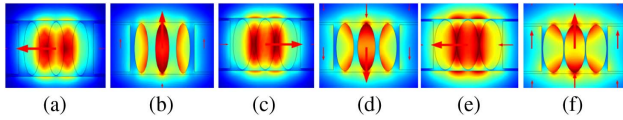


Fig. 3. Mode field distribution at 1.1 THz and different core air hole widths. (a) $b = 43 \mu\text{m}$, x-pol; (b) $b = 43 \mu\text{m}$, y-pol; (c) $b = 53 \mu\text{m}$, x-pol; (d) $b = 53 \mu\text{m}$, y-pol; (e) $b = 63 \mu\text{m}$, x-pol; (f) $b = 63 \mu\text{m}$, y-pol.

different from the y -polarization, which results in birefringence. The value of effective refractive index for the y -polarization is 1.20. Simulation of the PCF indicates that other modes may exist in the PCF, but for those other modes the electric fields will propagate through the cladding region. So, when a light pulse is allowed to follow through the waveguide, only the principal mode will be excited and hence the fiber will operate with a single mode [6].

Now, we characterize the property of birefringence with respect to frequency for different minor axis length (b) of elliptical air holes that is shown in Fig. 4. We have seen that birefringence increases with the reduction of b . It is also seen that birefringence increases with the increase of frequency. As the core air hole width decreases, the index difference between the x - and y -polarization modes increases, which causes the increment of birefringence.

The EML as a function of frequency and different (b) is shown in Fig. 5. It is observed that EML decreases with the increase of (b). The increase of (b) increases the amount of air and reduces the amount of material from the core, which causes the EML to be reduced. It is also observed that the EML increases with the increase of frequency. This phenomenon is true because it meets the theoretical consequences of calculating the material absorption loss with respect to frequency. The empirical equation of calculating EML is given by $\alpha(\nu) = \nu^2 + 0.63\nu - 0.13, \text{ cm}^{-1}$ [43]. It can also be seen that the EML in the y -polarization mode is less than in the x -polarization mode because from Fig. 3 it can be observed that in y polarization less light is transferred to the cladding region and the background material and a major portion of light passes through the core air holes.

From Figs. 4 and 5, it can be concluded that the highest amount of birefringence is obtained at $b = 43 \mu\text{m}$ and

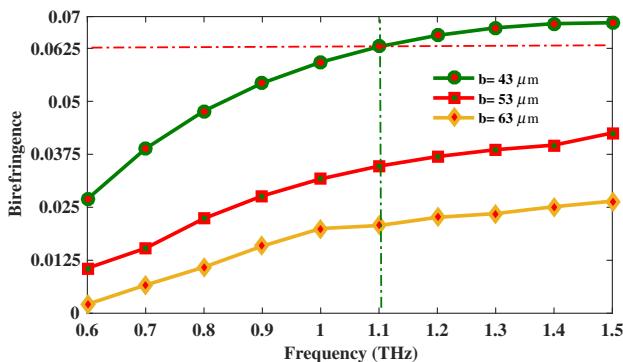


Fig. 4. Birefringence variation with respect to frequency at different minor axis length b .

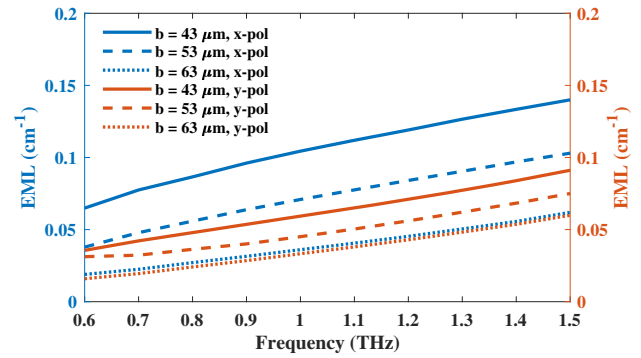


Fig. 5. EML versus frequency at different minor axis length of elliptical air holes (b) at both x - and y -polarization modes.

1.5 THz, and also the lowest amount of EML is obtained at 0.6 THz, $b = 63 \mu\text{m}$, and the y -polarization mode. However, one of the main considerations of our proposed PCF is birefringence, which is why we choose $b = 43 \mu\text{m}$ as the optimum minor axis length. We could reduce the value of b further, but that would gradually increase the EML of the fiber.

Moreover, using a typical fabrication tolerance of $\pm 2\%$ variation in global parameters of a PCF [6] and according to Figs. 4 and 5, there will be negligible impact of fabrication tolerance in the proposed fiber performance.

The amount of power transferring through the core region with the variation of frequency is shown in Fig. 6. It can be observed that core power increases with frequency up to 1.1 THz and then starts to decrease. This is because, at 1.1 THz, the fraction of mode power propagating through the core reaches its optimum, and a further increase of frequency causes the mode power to start to spread towards the cladding as well as the background material.

Therefore, comparing Fig. 5 and Fig. 6, it can be observed that a lower EML and higher core power fraction is experienced for the y -polarization over the x -polarization mode, and thus we choose the y -polarization mode as optimum. Moreover, from Fig. 6 it can be seen that the core power fraction reaches its maximum at 1.1 THz; thus we choose 1.1 THz as the operating frequency. Therefore, at optimum b , polarization mode, and frequency, the obtained birefringence, EML, and core

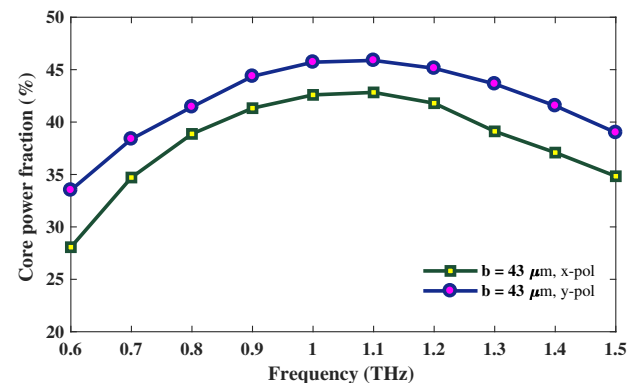


Fig. 6. Intensity of core power in the core region with respect to frequency at optimum b and orthogonal polarization mode.

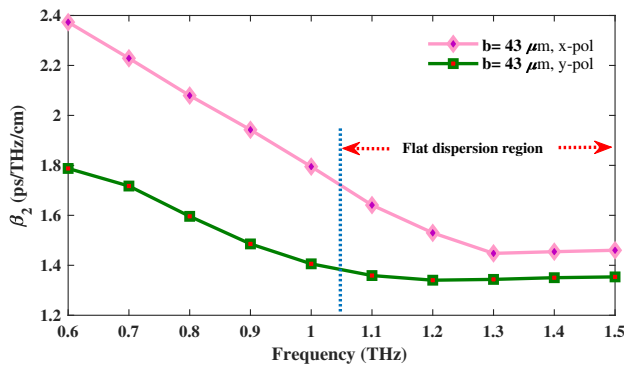


Fig. 7. Dispersion variation with respect to frequency at optimum b and orthogonal polarization modes.

power fraction are 0.063, 0.06 cm^{-1} , and 46%, which are improved over previously reported [35–43] terahertz waveguides.

In Fig. 7 the dispersion variation of the proposed PCF with respect to frequency is shown. From the characteristics, it is seen that there is a broad difference of dispersion values between the x - and y -polarization modes. This is true because the PCF structure is asymmetrical so the characteristics difference will be larger. We have seen that for x - and y -polarization modes the dispersion variations are $\pm 0.45 \text{ ps/THz/cm}$ and $\pm 0.23 \text{ ps/THz/cm}$ for the frequency range of 0.6–1.5 THz. However, we choose the bandwidth 1.05–1.5 THz in the y -polarization mode as the operating band because in that region the dispersion variation is $\pm 0.02 \text{ ps/THz/cm}$, which is the lowest for any proposed terahertz PCF. Note that the obtained dispersion value is suitable for multichannel communication applications, as dispersion limits information rate.

The characteristics of confinement loss with the variation of frequency are demonstrated in Fig. 8. It can be observed that confinement loss decreases with respect to frequency. This is because at higher frequencies the mode fields confine more tightly into the core region and hence the confinement loss reduces. At optimal design conditions the obtained confinement loss is $5.45 \times 10^{-13} \text{ cm}^{-1}$, which is trivial as compared to the obtained EML.

The area covered by the mode fields in the core air hole region is depicted through Fig. 9. It can be observed that

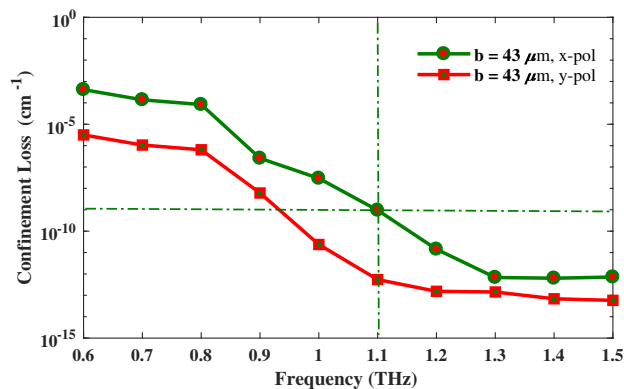


Fig. 8. Confinement loss versus frequency at optimum b and orthogonal polarization modes.

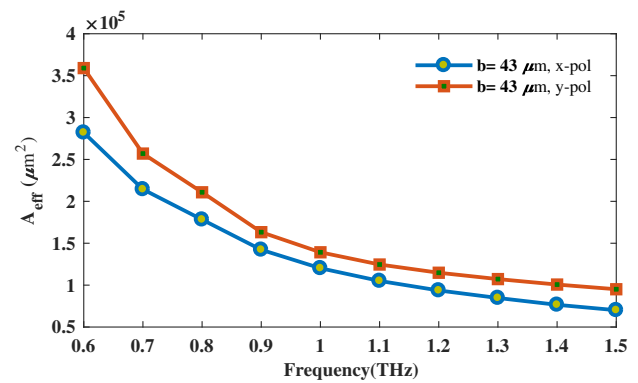


Fig. 9. Modal effective area versus frequency at 43 μm core air hole diameter and orthogonal polarization modes.

the effective area reduces with the increase of frequency. The physical reason is that at higher frequencies transverse mode fields are more tightly confined to the porous core region. At optimum design parameters, the obtained effective area is $1.20 \times 10^5 \text{ μm}^2$, which is comparable to the previously proposed [29–33] terahertz waveguides.

5. SCOPE OF EXPERIMENTAL CHARACTERIZATION OF THE PROPOSED ELLIPTICAL ARRAY BASED PCF

The experimental characterization procedure for all types of terahertz fibers is shown in Fig. 10. Using terahertz time domain spectroscopy (THz-TDS), the terahertz properties of fibers can be characterized [41,50]. A mode locked Ti:sapphire laser can be used to drive the emitter and detector of the THz-TDS. The emitter can be a photo-conductive antenna array [56], while the detector can be a dipole antenna. The fabricated fiber can be placed in between the emitter and detector. The fiber tip needs to be placed close to the emitter and detector. Here, the delay stage is used to enable sampling of terahertz pulses in the time domain.

Table 1 shows a comparison of characteristics between the proposed PCF and previously proposed terahertz PCFs. Our

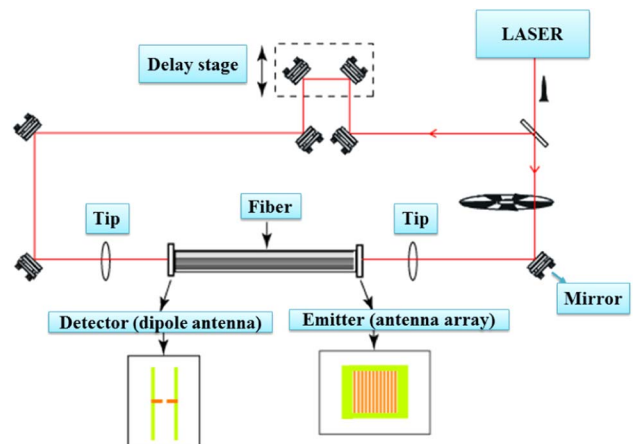


Fig. 10. Experimental setup procedure of the proposed PCF using THz-TDS [41,50].

Table 1. Comparison between the Obtained Result of the Proposed PCF and That of Other PCFs

Ref.	f (THz)	β_2 (ps/THz/cm)	B	$\alpha_{\text{eff}}(\text{cm}^{-1})$	$L_c(\text{cm}^{-1})$
[34]	1	± 0.5	0.075	0.07	0.034
[35]	1	± 1.42	0.048	0.085	4.40×10^{-4}
[36]	1	± 0.39	0.045	0.08	—
[37]	3	$0.2-1$	0.03	0.06	4.34×10^{-4}
[38]	1	—	0.019	0.0689	—
[39]	0.7	± 0.55	10^{-2}	0.07	4.34
[40]	0.5	± 0.5	—	0.0103	3.8
[43]	1	± 0.12	0.063	0.081	3.6×10^{-2}
This paper	1.1	± 0.02	0.063	0.06	5.45×10^{-13}

proposed PCF achieves improved terahertz characteristics over prior PCFs.

6. CONCLUSION

A novel Zeonex based near-zero dispersion flattened and highly birefringent PCF is designed and analyzed for potential application in the terahertz frequency band. The proposed fiber shows two promising properties: one is near-zero flat dispersion, and the other is high birefringence. The obtained near-zero dispersion flattened characteristics of ± 0.02 ps/THz/cm are suitable for multichannel communication application where different optical pulses experience nearly equal pulse broadening. Moreover, the high birefringence of 0.063 and low loss characteristics of the PCF are suitable for polarization preserving applications, especially for sensing and filtering. The commercial deployment of the fiber is achievable as it is feasible to fabricate with the existing fabrication technology. Therefore, it is anticipated that the proposed PCF will create a new window of opportunity for next generation terahertz research.

Funding. Australian Research Council (ARC) (DP170104984).

REFERENCES

- D. Abbott and X.-C. Zhang, "Scanning the issue: T-ray imaging, sensing, and resection," *Proc. IEEE* **95**, 1509–1513 (2007).
- J. Sultana, M. S. Islam, M. R. Islam, and D. Abbott, "High numerical aperture, highly birefringent novel photonic crystal fibre for medical imaging applications," *Electron. Lett.* **54**, 61–62 (2017).
- R. M. Woodward, V. P. Wallace, and D. D. Arnone, "Terahertz pulsed imaging of skin cancer in the time and frequency domain," *J. Biol. Phys.* **29**, 257–261 (2003).
- C. Yu and S. Fan, Y. Sun and E. Pickwell-MacPherson, "The potential of terahertz imaging for cancer diagnosis: a review of investigations to date," *Quant. Imaging Med. Surgery* **2**, 33–45 (2012).
- W. Withayachumnankul, G. M. Png, X. Yin, S. Atakaramians, I. Jones, H. Lin, B. S. Y. Ung, J. Balakrishnan, B. W.-H. Ng, B. Ferguson, S. P. Micken, B. M. Fischer, and D. Abbott, "T-ray sensing and imaging," *Proc. IEEE* **95**, 1528–1558 (2007).
- M. S. Islam, J. Sultana, K. Ahmed, A. Dinovits, M. R. Islam, B. W.-H. Ng, and D. Abbott, "A novel approach for spectroscopic chemical identification using photonic crystal fiber in the terahertz regime," *IEEE Sens. J.* **18**, 575–582 (2018).
- K. Kawase, Y. Ogawa, Y. Watanabe, and H. Inoue, "Non-destructive terahertz imaging of illicit drugs using spectral fingerprints," *Opt. Express* **11**, 2549–2554 (2003).
- T. Nagatsuma, G. Ducournau, and C. C. Renaud, "Advances in terahertz communications accelerated by photonics," *Nat. Photonics* **10**, 371–379 (2016).
- Md. S. Islam, J. Sultana, S. Rana, M. R. Islam, M. Faisal, S. F. Kaijage, and D. Abbott, "Extremely low material loss and dispersion flattened TOPAS based circular porous fiber for long distance terahertz wave transmission," *Opt. Fiber Technol.* **34**, 6–11 (2017).
- M. Mizuno, K. Fukunaga, S. Saito, and I. Hosako, "Analysis of calcium carbonate for differentiating between pigments using terahertz spectroscopy," *J. Eur. Opt. Soc. Rapid Publ.* **4**, 09044 (2009).
- K. I. Zaytsev, K. G. Kudrin, V. E. Karasik, I. V. Reshetov, and S. O. Yurchenko, "In vivo terahertz spectroscopy of pigmentary skin nevi: pilot study of non-invasive early diagnosis of dysplasia," *Appl. Phys. Lett.* **106**, 053702 (2015).
- C. B. Reid, A. Fitzgerald, G. Reese, R. Goldin, P. Tekkis, P. S. O'Kelly, E. Pickwell-MacPherson, A. P. Gibson, and V. P. Wallace, "Terahertz pulsed imaging of freshly excised human colonic tissues," *Phys. Med. Biol.* **56**, 4333–4353 (2011).
- P. C. Ashworth, E. Pickwell-MacPherson, E. Provenzano, S. E. Pinder, A. D. Purushotham, M. Pepper, and V. P. Wallace, "Terahertz pulsed spectroscopy of freshly excised human breast cancer," *Opt. Express* **17**, 12444–12454 (2009).
- R. H. Clothier and N. Bourne, "Effects of THz exposure on human primary keratinocyte differentiation and viability," *J. Biol. Phys.* **29**, 179–185 (2003).
- D. J. Cook, B. K. Decker, and M. G. Allen, "Quantitative THz spectroscopy of explosive materials," in *OSA Optical Terahertz Science and Technology Conference, USA* (2005), paper PSI-SR-1196.
- J. S. Drukteinis, B. P. Mooney, C. I. Flowers, and R. A. Gatenby, "Beyond mammography: new frontiers in breast cancer screening," *Am. J. Med.* **126**, 472–479 (2013).
- H. Cheon, H. J. Yang, and J. H. Son, "Toward clinical cancer imaging using terahertz spectroscopy," *IEEE J. Sel. Top. Quantum Electron.* **23**, 1–9 (2017).
- P. H. Siegel, "Terahertz technology," *IEEE Trans. Microwave Theor. Tech.* **50**, 910–928 (2002).
- J. Mullins, "Using unusable frequencies solid-state terahertz laser," *IEEE Spectrum* **39**, 22–23 (2002).
- S. Atakaramians, S. Afshar, V., T. M. Monro, and D. Abbott, "Terahertz dielectric waveguides," *Adv. Opt. Photon.* **5**, 169–215 (2013).
- N. N. Chen, J. Liang, and L. Y. Ren, "High-birefringence, low-loss porous fiber for single-mode terahertz-wave guidance," *Appl. Opt.* **52**, 5297–5302 (2013).
- K. Wang and D. M. Mittleman, "Metal wires for terahertz waveguiding," *Nature* **432**, 376–379 (2004).
- B. Bowden, J. A. Harrington, and O. Mitrofanov, "Silver/polystyrene coated hollow glass waveguides for the transmission of terahertz radiation," *Opt. Lett.* **32**, 2945–2947 (2007).
- L.-J. Chen, H. Chen, T. Kao, J. Lu, and C. Sun, "Low loss sub-wavelength plastic fiber for terahertz wave guiding," *Opt. Lett.* **31**, 308–310 (2006).
- M. Skorobogatiy and A. Dupuis, "Ferroelectric all-polymer hollow Bragg fibers for terahertz guidance," *Appl. Phys. Lett.* **90**, 113514 (2007).
- G. Zhao, M. T. Mors, and T. Wenckebach, "Terahertz dielectric properties of polystyrene foam," *J. Opt. Soc. Am. B* **19**, 1476–1479 (2002).
- A. Hossain and Y. Namihiro, "Light source design using Kagome lattice hollow core photonic crystal fibers," *Opt. Rev.* **21**, 490–495 (2014).
- D. Pristinski and H. Du, "Solid-core photonic crystal fiber as a Raman spectroscopy platform with a silica core as an internal reference," *Opt. Lett.* **31**, 3246–3248 (2006).
- J. Sultana, Md. S. Islam, J. Atai, M. R. Islam, and D. Abbott, "Near-zero dispersion flattened, low-loss porous-core waveguide design for terahertz signal transmission," *Opt. Eng.* **56**, 076114 (2017).
- Md. S. Islam, J. Sultana, J. Atai, M. R. Islam, and D. Abbott, "Design and characterization of a low-loss, dispersion-flattened photonic crystal fiber for terahertz wave propagation," *Optik* **145**, 398–406 (2017).
- M. S. Islam, S. Rana, M. R. Islam, M. Faisal, H. Rahman, and J. Sultana, "Porous core photonic crystal fiber for ultra-low material loss in THz regime," *IET Commun.* **10**, 2179–2183 (2016).

32. S. Islam, M. R. Islam, M. Faisal, A. S. M. S. Arefin, H. Rahman, J. Sultana, and S. Rana, "Extremely low-loss, dispersion flattened porous-core photonic crystal fiber for terahertz regime," *Opt. Eng.* **55**, 076117 (2016).
33. M. S. Islam, J. Sultana, J. Atai, D. Abbott, S. Rana, and M. R. Islam, "Ultra low-loss hybrid core porous fiber for broadband applications," *Appl. Opt.* **56**, 1232–1237 (2017).
34. R. Islam, M. S. Habib, G. K. M. Hasanuzzaman, R. Ahmad, S. Rana, and S. F. Kaijage, "Extremely high-birefringent asymmetric slotted-core photonic crystal fiber in THz regime," *IEEE Photonics Technol. Lett.* **27**, 2222–2225 (2015).
35. M. R. Hasan, Md. S. Anower, Md. A. Islam, and S. M. A. Razzak, "Polarization-maintaining low-loss porous-core spiral photonic crystal fiber for terahertz wave guidance," *Appl. Opt.* **55**, 4145–4152 (2016).
36. R. Islam, Md. S. Habib, G. K. M. Hasanuzzaman, S. Rana, and Md. A. Sadath, "Novel porous fiber based on dual-asymmetry for low-loss polarization maintaining THz wave guidance," *Opt. Express* **41**, 440–443 (2016).
37. Z. Wu, Z. Shi, H. Xia, X. Zhou, Q. Deng, J. Huang, X. Jiang, and W. Wu, "Design of highly birefringent and low-loss oligoporous-core THz photonic crystal fiber with single circular air-hole unit," *IEEE Photonics J.* **8**, 4502711 (2016).
38. K. Ahmed, S. Chowdhury, B. K. Paul, Md. S. Islam, S. Sen, Md. I. Islam, and S. Asaduzzaman, "Ultrahigh birefringence, ultralow material loss porous core single-mode fiber for terahertz wave guidance," *Appl. Opt.* **56**, 3477–3483 (2017).
39. R. Islam, M. S. Habib, G. K. M. Hasanuzzaman, S. Rana, M. A. Sadath, and C. Markos, "A novel low-loss diamond-core porous fiber for polarization maintaining terahertz transmission," *IEEE Photonics Technol. Lett.* **28**, 1537–1540 (2016).
40. S. Rana, A. S. Rakin, H. Subbaraman, R. Leonhardt, and D. Abbott, "Low loss and low dispersion fiber for transmission applications in the terahertz regime," *IEEE Photonics Technol. Lett.* **29**, 830–833 (2017).
41. S. Atakaramians, S. A. Vahid, M. Nagel, H. Ebendorff-Heidepriem, B. M. Fischer, T. M. Monro, and D. Abbott, "Experimental investigation of dispersion properties of THz porous fibers," in *34th International Conference on Infrared, Millimeter, and Terahertz Waves*, Busan (2009), pp. 1–2.
42. S. Atakaramians, S. Afshar, V., B. M. Fischer, D. Abbott, and T. M. Monro, "Low loss, low dispersion and highly birefringent terahertz porous fibers," *Opt. Commun.* **282**, 36–38 (2009).
43. J. Luo, F. Tian, H. Qu, L. Li, J. Zhang, X. Yang, and L. Yuan, "Design and numerical analysis of a THz square porous-core photonic crystal fiber for low flattened dispersion, ultrahigh birefringence," *Appl. Opt.* **56**, 6993–7001 (2017).
44. W. C. Tay and E. L. Tan, "Implementations of PMC and PEC boundary conditions for efficient fundamental ADI-and LOD-FDTD," *J. Electromagn. Waves Appl.* **24**, 565–573 (2010).
45. C. S. Ponceca, R. Pobre, E. Estacio, N. Sarukura, A. Argyros, M. C. Large, and M. A. van Eijkelenborg, "Transmission of terahertz radiation using a micro-structured polymer optical fiber," *Opt. Lett.* **33**, 902–904 (2008).
46. M. Goto, A. Quema, H. Takahashi, S. Ono, and N. Sarukura, "Teflon photonic crystal fiber as terahertz waveguide," *Jpn. J. Appl. Phys.* **43**, L317–L319 (2004).
47. G. Woyessa, A. Fasano, C. Markos, A. Stefani, H. K. Rasmussen, and O. Bang, "Zeonex microstructured polymer optical fiber: fabrication friendly fibers for high temperature and humidity insensitive Bragg grating sensing," *Opt. Mater. Express* **7**, 286–295 (2017).
48. X. Tang, Y. Jiang, B. Sun, J. Chen, X. Zhu, P. Zhou, D. Wu, and Y. Shi, "Elliptical hollow fiber with inner silver coating for linearly polarized terahertz transmission," *IEEE Photonics Technol. Lett.* **25**, 331–334 (2013).
49. Babita and V. Rastogi, "Dispersion flattened single mode optical fiber with large effective area," *AIP Conf. Proc.* **1536**, 729–730 (2013).
50. S. Atakaramians, S. Afshar, V., H. Ebendorff-Heidepriem, M. Nagel, B. M. Fischer, D. Abbott, and T. M. Monro, "THz porous fibers: design, fabrication and experimental characterization," *Opt. Express* **17**, 14053–14062 (2009).
51. N. A. Issa, M. A. van Eijkelenborg, M. Fellow, F. Cox, G. Henry, and M. C. J. Large, "Fabrication and study of microstructured optical fibers with elliptical holes," *Opt. Lett.* **29**, 1336–1338 (2004).
52. F. Liu, H. Gao, Q. Xu, and Y. Zhang, "Fabrication and characteristics of elliptical-holes and near elliptical core hexangular lattice photonic crystal fibers based on polymer," *Adv. Mater. Res.* **279**, 151–156 (2011).
53. J. Sultana, Md. S. Islam, M. Faisal, M. R. Islam, B. W.-H. Ng, H. Ebendorff-Heidepriem, and D. Abbott, "Highly birefringent elliptical core photonic crystal fiber for terahertz application," *Opt. Commun.* **407**, 92–96 (2017).
54. H. Ebendorff-Heidepriem and T. M. Monro, "Extrusion of complex preforms for microstructured optical fibers," *Opt. Express* **15**, 15086–15092 (2007).
55. H. Ebendorff-Heidepriem, J. Schuppich, A. Dowler, L. Lima-Marques, and T. M. Monro, "3D-printed extrusion dies: a versatile approach to optical material processing," *Opt. Mater. Express* **4**, 1494–1504 (2014).
56. M. Wachter, M. Nagel, and H. Kurz, "Metallic slit waveguide for dispersion-free low-loss terahertz signal transmission," *Appl. Phys. Lett.* **90**, 061111 (2007).